Feasibility study of using the dispersion of surface acoustic wave impulse for viscoelasticity characterization in tissue mimicking phantoms

Zhou, Kanheng; Li, Chunhui; Chen, Siping; Nabi, Ghulam; Huang, Zhihong

Published in:
Journal of Biophotonics

DOI:
10.1002/jbio.201800177

Publication date:
2019

Document Version
Peer reviewed version

Feasibility study of using the dispersion of surface acoustic wave (SAW) impulse for viscoelasticity characterization in tissue mimicking phantoms

Kanheng Zhou[1], Chunhui Li[1]*, Siping Chen[2], Ghulam Nabi[3] and Zhihong Huang[1]

[1] School of Science and Engineering, University of Dundee;
[2] School of Biomedical Engineering, Shenzhen University;
[3]School of Medicine, University of Dundee;
*Correspondence: c.li@dundee.ac.uk; Tel.: +44-1380-287-6730

Abstract: The aim of this study was to investigate the feasibility of utilizing the phase velocity dispersion of impulse surface acoustic wave (SAW) for viscoelasticity characterization of soft materials. The focused ultrasound transducer and the phase sensitive optical coherence tomography (PhS-OCT) were applied as the impulse SAW inducer and tracker respectively. Three types of liquid-paraffin-based cream-in-agar phantoms were tested. Phase velocity dispersion curve was extracted using a Fourier transform based phase velocity analysis algorithm. Viscoelastic parameters were obtained by fitting the dispersion curve of SAW into Rayleigh wave dispersion equation. The estimated viscoelasticity was compared with that from spherical indenter, ramp-hold relaxation testing for validation. Both results show an increasing trend in the elasticity and decreasing trend in the viscosity with the concentration of liquid-paraffin-based cream increasing in the samples. The proposed method has the capability of evaluating the viscoelastic properties of homogeneous soft tissue. By combining viscoelastic parameters estimated from the proposed method, the dispersive-SAW-impulse-based viscosity compensated elastography could be further developed.

Keywords: viscoelasticity; impulse surface acoustic wave; dispersion; tissue mimicking phantoms; phase velocity; load-relaxation test

1. Introduction

Elasticity and viscosity of biological tissue are important properties in medicine because they are closely correlated with pathological conditions. For example, Young's modulus of disease tissue in prostate, breast and skin can be much higher than the surrounding normal tissue. Typically, prostate tumor is ~2 times stiffer than the normal anterior/posterior tissue, the breast tumor is ~10 - ~20 times stiffer than the normal fat/glandular tissue, and skin of scleroderma patient is ~ 2 -3 times stiffer than the skin of health person at the same position [1, 3]. On the other hand, viscosity of liver, which can be determined by the dispersion degree of shear wave speed, increases with the growth in the degree of liver steatosis [2]. In Systemic Sclerosis (SSc), there is evidence showing the skin viscosity of SSc patient is ~ 1.5 – 3 times higher than that in control group, e.g. health people, and the skin viscosity increases with the growth of extent of skin involvement in SSc [3-4]. In addition, it has also been proven that the correct estimation of viscosity is important for accurately estimating true tissue elasticity. The shear modulus of oil-in-gelatin phantom could be overestimated ~100% if the pure elastic model is applied, i.e. ignoring the dispersive effect of the shear waves and using the shear wave group velocity to estimate the elasticity [5]. Thus, taking viscosity into account is necessary for accurate characterization biological soft tissue for aiding disease diagnosis.

Many techniques have been developed to measure the soft tissue viscoelastic property in the past two decades, including indentation test (quasi-static), dynamic mechanical analysis (DMA,

This article has been accepted for publication and undergone full peer review but has not been through the copyediting, typesetting, pagination and proofreading process, which may lead to differences between this version and the Version of Record. Please cite this article as doi: 10.1002/jbio.201800177

dynamic), and shear wave ultrasound vibrometry (SDUV, wave dispersion) [6-8]. All these methods measure the response of soft tissue to an excitation force, whether the force is excited quasi-statically by compression [6], dynamically by vibration [9] or internally by ultrasound acoustic radiation force [5]. The response of soft tissue is then fitted into different rheological model (Maxwell model [10], Kelvin-Voigt model [11], standard linear solid model [12] or Kelvin-Voigt fractional derivative (KVFD) model [6]) or shear wave dispersion equation [5, 9] to infer viscoelastic properties. Among them, SDUV attracts a wide range of interests because it is convenient to implement with a clinical ultrasound system [8]. SDUV estimates the viscoelasticity through obtaining the shear wave phase velocities over a frequency range (from 0 Hz to 1 kHz) deep inside the tissue, and then fitting the data into a shear wave dispersion model [8]. Currently, SDUV has already been applied to estimate the viscoelasticity of various types of soft tissue, including liver, prostate and kidney [8]. An in-vivo experiment in porcine liver showed the viscoelasticity evaluated by SDUV was in good agreement with that from MRE studies on normal human and rat livers [13]. The elasticity and viscosity estimated using SDUV on three freshly excised human prostates fell within the range found in normal prostates using other methods, including sonoelastography, acoustic radiation force imaging (ARFI) and magnetic resonance elastography (MRE) [14-17]. SDUV has also been applied to precisely characterize the viscoelasticity of the cortex of *ex-vivo* porcine kidney (coefficient of variation defined by stand deviation over mean value is less than 1%), and the results agree with that from MRE [18]. However, it is difficult to generate pure shear wave in the superficial area that is within 2 mm under the surface, whether in contact manner by mechanical shaker or in remote manner by focused ultrasound transducer or phase array ultrasound transducer. The wave generated by either of the method is a combination of the shear wave inside the sample and the surface acoustic wave (SAW) on the surface. Hence, this technique has the limitation in superficial application, e.g. skin disease diagnosis and endoscope-based tissue characterization.

To evaluate the viscoelasticity of the superficial area of biological tissue, it is better to use SAW instead of shear wave since the main energy of SAW is remained on sample surface. Besides, it is easy to generate SAW on the free sample surface using mechanical shaker [19], high energy laser [20] or focused ultrasound transducer [21]. Compared to ultrasound sensors, phase sensitive optical coherence tomography (PhS-OCT) system has a higher spatial resolution (typically 8 ~ 15 μm), and the probing depth can reach up to ~ 3 mm, which meets our requirements. The previous work in our group has already demonstrated the capability of surface acoustic wave based optical coherence elastography (SAW-OCE) for elasticity evaluation of homogeneous / heterogeneous tissue mimicking phantoms, *ex-vivo* porcine skin, and *in-vivo* human skin [19, 21]. However, we ignored the viscosity of the medium and use linear elastic module to evaluate the Young's modulus of the sample. To further improve the current technique and evaluate the viscoelasticity of biological tissue, the impulse SAW dispersion data was required to be fitted into the Rayleigh wave dispersion equation for extracting both shear elasticity μ_1 and shear viscosity μ_2.

There had been a number of attempts to evaluate the viscoelasticity of biological tissue using the dispersion of Rayleigh wave recently. Zhang *et. al.* demonstrated their surface-wave-based viscoelasticity estimation technique using shaker-laser-vibrometer system in scleroderma [3]. Han *et. al.* briefly reported their Rayleigh wave viscoelasticity characterization approach using air-puff OCE system and demonstrated their method in oil-in-gelatin phantom and in in-vitro chicken liver [22]. Chen *et. al.* reported their method for estimating both elasticity and viscosity of soft tissue based on

laser speckle contrast imaging (LSCI) and approximate Rayleigh wave dispersion formula. They also demonstrated their method in oil-in-gelatin phantom [23].

In this study, we reported a novel method that combines conventional SAW-OCE setup to acquire impulse SAW dispersion data and Rayleigh wave dispersion equation to simultaneously estimate both elasticity and viscosity of the sample. This study aims to: 1) overcome the limitation of SDUV in superficial applications; 2) improve current SAW-OCE technique to characterize the viscoelasticity of biological tissue/tissue mimicking material using the dispersion of impulse SAW. 10%, 20% and 30% liquid-paraffin-based cream-in-agar phantoms were tested. Liquid-paraffin-based cream was added into the agar solution for changing the viscosity of phantom without significantly changing the phantom stiffness [6]. The impulse SAW was generated by a customized miniature focused ultrasound (FUS) transducer, and the wave propagation was captured by a phase-sensitive optical coherence tomography system. The impulse SAW dispersion curve was then derived using a 2D fast Fourier transform based phase velocity analysis algorithm. The shear elasticity μ_1 and shear viscosity μ_2 were finally obtained after fitting dispersion curve into Rayleigh wave dispersion equation. An independent spherical indenter, ramp-hold relaxation test was performed in the end for cross-validation purpose.

2. Theoretical Background

2.1 Surface acoustic wave impulse dispersion in viscoelastic materials

When a material is stimulated by an impulse, various kinds of mechanical pressure waves are generated within the material simultaneously, including longitudinal waves, shear waves in the material and surface acoustic waves (Rayleigh wave) on the sample-air inter surface.

In a viscoelastic, isotropic and homogeneous material (Kelvin-Voigt medium), the propagation of the surface acoustic wave shows a dispersion behavior, in which different frequency components have different phase velocities. The dispersion equation of surface acoustic wave (Rayleigh wave) can be expressed as follows based on the wavenumbers [24]:

$$4{k_R}^3\sqrt{k_R^2-k_s^2}-(k_s^2-2k_R^2)^2-\frac{\rho_{air}}{\rho_{sample}}k_s^4=0, \tag{1}$$

$$k_R=\frac{\omega}{C_R(\omega)}, \tag{2}$$

$$k_s=\omega\sqrt{\frac{\rho_{sample}}{\mu_1+i\omega\mu_2}}, \tag{3}$$

Here, k_R is the surface acoustic wave number, k_s is the shear wave number, ω is the angular frequency, $C_R(\omega)$ is the phase velocity of surface acoustic wave, ρ_{air} is the density of air, ρ_{sample} is the density of the sample, μ_1 and μ_2 are the shear elasticity and shear viscosity, respectively. Therefore, the viscoelasticity μ_1 and μ_2 of an unknown material can be evaluated if the surface acoustic wave dispersion can be measured in that material.

2.2 Spherical indenter, ramp-hold relaxation solution based on Kelvin-Voigt fractional derivative (KVFD) model

Load-relaxation test is a highly recognized, reliable, direct material test modality for characterizing the mechanical properties for a large variety of materials. Most load-relaxation tests utilize the step-hold relaxation response of the material to estimate the mechanical properties. However, it has difficulty in applying a near-step strain without generating oscillations that would induce significant error in model fitting [6]. In contrast, ramp-hold relaxation response avoids measurement artefacts (e.g. oscillations) and dramatically improves model-fit stability [25-26].

The KVFD model is employed in this ramp-hold relaxation test to describe the time-dependent relaxation behaviour of viscoelastic biological tissue since fractional derivative models could represent viscoelastic behaviour more closely than integer-order models with fewer parameters [27-28].

The force relaxation on the probe is keeping monitoring over time when the spherical indenter tip is pressed onto the surface of large-size samples (the diameter of the sample is ten times larger than the diameter of the indenter) at a constant speed and held fixed at final position. The time-varying force response during the ramp-hold relaxation test can be expressed as follows [6]:

$$P_r(t) = \begin{cases} 4E_0\sqrt{R(kt)^3}\left[\frac{2}{3} + \frac{\left(\frac{t}{\tau}\right)^{-\alpha}}{\Gamma(1-\alpha)} B\left(\frac{3}{2}, 1-\alpha\right)\right], & 0 < t \le T_r \\ 4E_0\sqrt{R(kT_r)^3}\left[\frac{2}{3} + \frac{\left(\frac{t}{T_r}\right)^{\frac{3}{2}}\left(\frac{t}{\tau}\right)^{-\alpha}}{\Gamma(1-\alpha)} B\left(\frac{T_r}{t}; \frac{3}{2}, 1-\alpha\right)\right], & t \ge T_r \end{cases} \quad (4)$$

where $P_r(t)$ is the time-varying force on the probe, R is the radius of spherical indenter, k is the speed of the spherical indenter tip, T_r is the duration of the ramp, $\Gamma(z) = \int_0^\infty e^{-t}t^{z-1}dt$ is a Gamma function, $B(x,y) = \int_0^1 t^{x-1}(1-t)^{y-1}dt \quad Re(x) > 0, Re(y) > 0$ is a complete beta function and $B(a;x,y) = \int_0^a t^{x-1}(1-t)^{y-1}dt$ for $a \in [0,1]$ is an incomplete beta function [6]. The elastic modulus E_0, derivative order α and relaxation time constant τ can be estimated by fitting the ramp-hold force relaxation curve into this equation. Then, the viscoelasticity of the material can be represented using the elastic modulus E_0, time-dependent viscosity $\eta = E_0 \cdot \tau^\alpha$ and the normalized viscosity coefficient $\eta_n = \tau^\alpha$.

3. Materials and Methods

3.1. Tissue mimicking phantom samples

10%, 20%, 30% liquid-paraffin-based cream in homogeneous 0.5% agar phantom (%wt) were employed as different viscoelastic tissue mimicking phantom samples in this study. 0.5%wt agar solution was firstly made by mixing agar powder (Merck Millipore, Germany) and degassed water in a sealed beaker at 95°C for 30 mins. Cream (Doublebase, UK) of different weight was added to visually clear agar solution after the agar solution was cooled down to 40 °C. The mixture was then stirred until it became visibly homogeneous using a mixer. All the samples were made in the same batch using different molds. The mold size for impulse SAW dispersion experiment was 50 mm in diameter and 5.5 mm in height, while the mold size for spherical indenter and ramp-hold relaxation experiment was 90mm in diameter and 12 mm in height respectively. All sample surfaces were flat and smooth. For impulse SAW dispersion experiment, each kind of phantom has 3 samples and each sample was repeatedly tested for 5 times in different locations. For spherical indenter, ramp-hold relaxation experiment, each kind of phantom has 3 samples and each sample was repeatedly tested in 5 different locations.

3.2 Impulse SAW dispersion experiment

3.2.1 Experimental setup

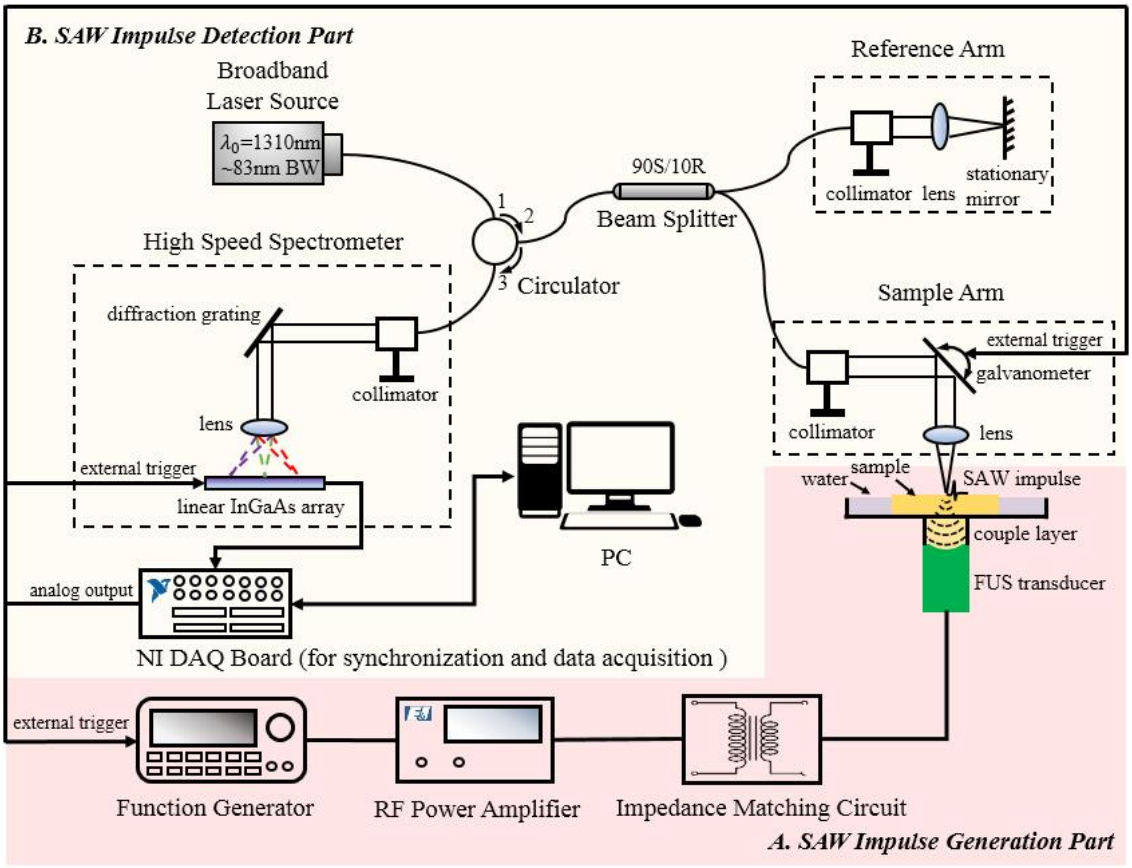

Figure 1. Setup for impulse SAW dispersion experiment. The FUS transducer is driven by an external triggered function generator, and works as a mechanical wave inducer (A, pink part). The synchronized PhS-OCT works as the mechanical wave detector (B, yellow part).

The setup for impulse SAW dispersion experiment (as shown in Figure 1) consisted of two parts: the impulse SAW generation part and the detection part. An impedance matched customized FUS transducer driven by an external triggered function generator (Keysight Technologies Inc., USA) and RF power amplifier (Electronics & Innovation, Ltd., USA), was used to generate impulse SAW. The driving signal was 1.0 Vpp sinewave burst with 100 cycles per pulse at FUS transducer working frequency, and the duration of the burst was 54 μs. The corresponding spatial-average time-average acoustic intensity at the focus was calculated to be 20mW/cm^2, which was much less than the typical diagnostic ultrasound intensity of 720 mW/cm^2 according to United States Food and Drug Administration (USFDA) regulations [30]. The distance between the FUS transducer and the sample surface equalled to the focal length of the transducer. Thus, the acoustic radiation force at FUS transducer focus on the sample-air interface introduced the SAW (mainly Rayleigh wave). The sample and FUS transducer were coupled through a couple layer made by the same material as the sample. The water around the sample was used to reduce the reflection of the generated mechanical wave from the edge of the sample. The induced impulse SAW was tracked by a synchronized PhS-OCT system and the data was acquired by LabVIEW program for post-processing.

3.2.2 Miniature FUS transducer

The customized miniature FUS transducer employed in this study has 1.488 MHz working frequency, 20 mm aperture, and 16 mm radius curvature. The impedance of the transducer was matched to 50 Ω for meeting the RF power transmission requirement. 2D normalized pressure field maps along radial and axial direction, shown in Figure 2(a-b), were created using a 500 μm diameter hydrophone (Precision Acoustics Ltd, UK). The dimension of focal zone was determined by full-width-half-maximum (FWHM) of both pressure field maps, and the size was ~7.74 mm × ~0.55 mm (axial × radial). Hence, the axial length was long enough to cover the imaging depth of PhS-OCT system (traditionally 3 mm maximum). Output acoustic power of the FUS transducer in water was calibrate using a radiation force balance (Precision Acoustic Ltd, UK). The output acoustic power increased from 0.5 W to 9.8 W when the driving voltage on function generator increased from 0.5 Vpp to 1.5 Vpp, which is shown in Figure 2(c). The driving voltage applied in this study was 1.0 Vpp, thus the output acoustic power was 2.874 W.

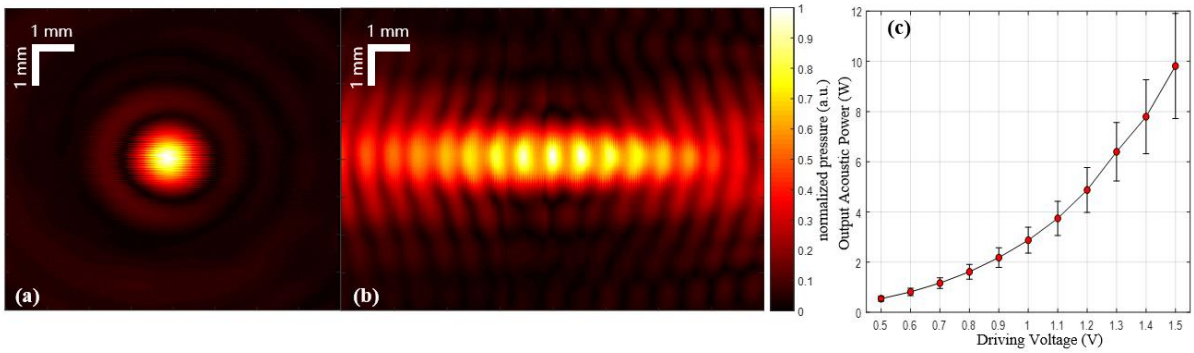

Figure 2. Normalized pressure field maps of the miniature FUS transducer along radial direction (a) and axial direction (b). The focal zone is elliptical shape with ~7.74 mm in length and ~1.1 mm in width.

3.2.3 Phase-sensitive optical coherence tomography system (PhS-OCT)

The PhS-OCT system applied in this study was a spectral-domain OCT (SD-OCT) system. The schematic diagram of this system is shown in Figure 1(B), which consists of a broadband super-luminescent diode (1310 nm central wavelength, ~83 nm bandwidth, 10 mW power, Thorlabs Inc., USA), a beam splitter, a stationary reference arm, a sample arm (integrated with a 2D galvo-scanner, Thorlabs Inc., USA) and a high-speed spectrometer (linear InGaAs camera, 46.8kHz working frequency, 17.4 μs exposure time, 450 e/count sensitivity, Sensors Unlimited Inc., USA). The PhS-OCT system does structure imaging by repeatedly detecting the intensity of the resulting spectral interferogram changing with its corresponding wavelength (A-line scan) along the lateral direction. The axial and lateral resolution of the system in the sample was ~9.1 μm and ~14.2 μm, respectively. In addition, the axial displacement at a given location $u_z(x,z,t)$ can also be calculated from the phase difference $\Delta\varphi(x,z,t)$ between two consecutive A-line scans at that location using the following equation [29]:

$$u_z(x,z,t) = \frac{\Delta\varphi(x,z,t) * \lambda}{4\pi n}, \tag{7}$$

where λ is the central wavelength of broadband light source, n is the refractive index of the medium. The phase sensitivity of the system in the sample is ~0.06 rad, corresponding to ~5 nm axial displacement.

3.2.4 Scanning protocol

To track the propagation of generated impulse SAW, the PhS-OCT system was operated in M-B scan mode, shown in Figure 3, and synchronized with the wave generation part at each M-scan using an external TTL trigger signal. Each M-scan consists of 512 A-scans acquired in the same location at the sampling frequency of 46.8 kHz. 512 M-scans repeated horizontally at 60 fps across the imaging plane forming one complete M-B scan, taking about 8.54 s. The data format for one complete M-B scan is 1024 pixel-depth (axial) × 512 M-scans (lateral) × 512 A-scans (time frames), and the size of effective imaging plane is ~2.2 mm × ~7.3 mm (depth × lateral distance).

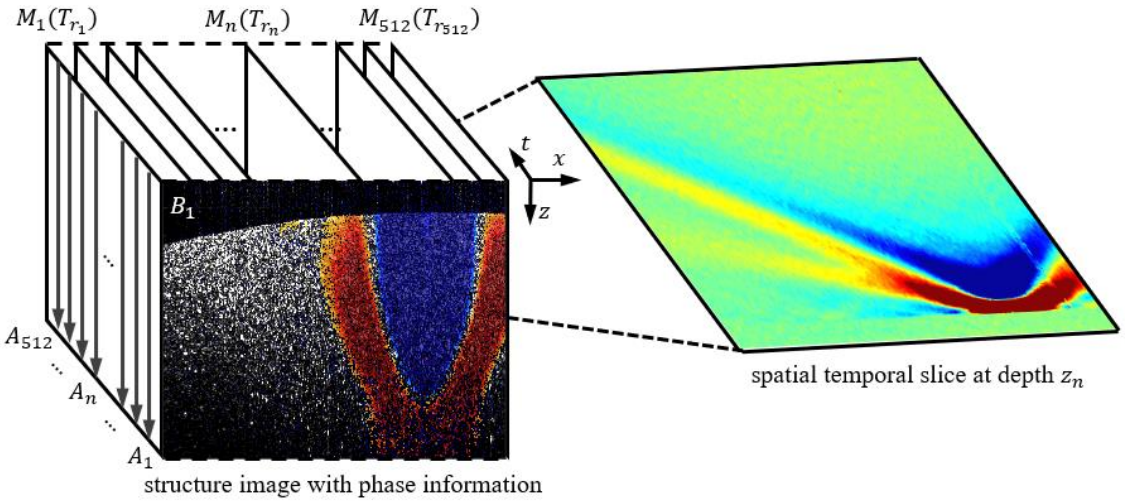

Figure 3. Illustration of PhS-OCT system scanning protocol for impulse SAW dispersion experiment. To track wave propagation, the system works at M-B scan mode. Each M-scan consists of 512 A-scans, and 512 M-scans forms one complete M-B scan. PhS-OCT and FUS transducer synchronizing trigger signal was repeatedly sent for each M-scan.

3.2.5 Data processing

A Fourier transform based phase velocity estimation algorithm was applied to extract the phase velocity dispersion curve in this study, described in detail in previous work [21]. Briefly, the phase velocity estimation starts from an unwrapped spatial temporal slice (Figure 3, right) were extracted from the sample surface. Then, a 2D fast Fourier transform was applied to convert the spatial temporal slice from space-time domain into wavenumber-frequency domain (k-f domain). After calculating the phase velocities for each frequency using equation 8 [31], the phase velocity intensity map was thus created by relating phase velocities with their corresponding intensity index. Finally, the phase velocity dispersion curve was obtained by selecting the phase velocities with maximal intensity for each frequency.

$$C_p(f) = \frac{f}{k_L}, \tag{8}$$

Here, $C_p(f)$ is the phase velocity of frequency f, k_L is the wavenumber.

To estimate the viscoelastic parameters of the material, the obtained phase velocity dispersion curves were then iterated into the wave dispersion models (Equation 2 for surface acoustic wave, Equation 6 for shear wave, ρ was measured to be 1100 kg/m^3 in this study). The MATLAB nonlinear least squares curve fitting tool was employed to do the curve fitting in this study.

3.3 Spherical indenter, ramp-hold relaxation test

The experiment setup for the spherical indenter, ramp-hold relaxation test is shown in Figure 4. It was implemented on Tinius Olsen H5KS material test machine (Tinius Olsen Ltd., UK) with a spherical-tipped aluminium indenter (8 mm diameter) at room temperature. A 10 N load cell was applied to do this experiment. The spherical indenter has a diameter less than one tenth of the sample diameter to minimize boundry effects [6]. The maximum displacement of the spherical tip into the sample surface was 0.6 mm (5% strain, 12 mm height). The compression speed was set to be 1 mm/min. Thus, the ramp time T_r was calculated to be 36 s, which is long enough (> 10 s) to obtion stable estimated model parameters. The indenter was held fixed for 300s after it reached the maximum displacement. The decaying force on the indenter was kept measuring by the load cell and kept recording by the Tinius Olsen Horizon software. The force-displacement data acquired was then imported into MATLAB for KVFD model fitting.

Figure 4. Setup for spherical indenter, ramp-hold relaxation test. It was implemented on a Tinius Olsen H5KS material test machine with an 8 mm diameter spherical-tipped aluminium indenter.

4. Results and Discussion

4.1. Impulse SAW propagation in tissue mimicking material

The snapshots in Figure 5(a-f) show the propagation of a tyical impulse SAW in a 20% cream-in-agar phantom at different time steps. The wave source was located on the right part of the sample. The wavefront of the impulse SAW can been seen clearly in each frame and wave propagation are also denoted in all frames by dark red arrows. The impulse SAW propagated horizontally along the air-phantom interface on both sides of the FUS focal sopt. Figure 5(g) shows the corresponding spectrum of the impulse SAW, which indicates the captured impulse SAW is broadband. The frequency range of this impulse was from DC to 1.5 kHz with above -30dB signal-to-noise ratio.

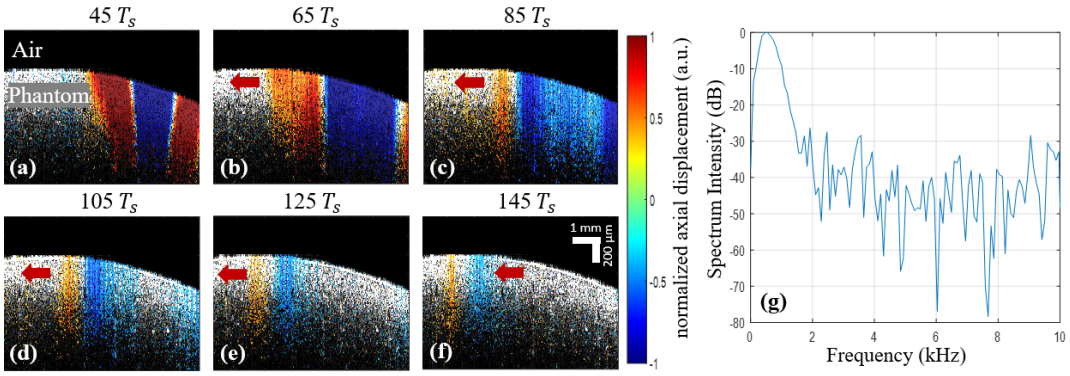

Figure 5. (I) Snapshots of impulse SAW propagation in 20% cream in 0.5% agar phantom at different time steps (*Ts* is the sampling period). Normalized axial displacements (color scale) are superimposed on structure images (gray scale) in all frames. The wave source is located on the right close to the edge, and the SAW propagation direction is denoted by small yellow arrows in each frame. The size of each frame is ~2.5 mm in depth × ~7 mm in lateral. (II) Spectrum of impulse SAW. The impulse has a frequency range of 0 ~ 1.5 kHz with about ~ -30 dB signal-to-noise ratio.

The unwrapped impulse SAW spatial-temporal slice extracted from the sample surface is shown in Figure 6(a). There were two wave propagation pathes in this unwrapped spatial-temporal slice. The wave with higher speed (marked as blue dash line) only existed in the initial 2 ms was the combination of different kinds of mechanial wave impulse (under sampled compressional wave and shear wave). While the wave with lower speed (highlighted by red dash line) was the pure impulse SAW that propagated from stimulation point to the sample edge. The wave profile of pure impulse SAW at different distances away from the wave source can be clearly observed by figure 6(b). The dispersion behaviour of impulse SAW can be noticed as the peaks at far field signals were broader than that at near field signals in the shape, it was expected in viscoelastic materials. The impulse SAW k-f domain image (figure 6(c)) described the frequency composition of the signal with corresponding intensity. It was obtained by appling 2D fast fourier transfrom (FFT) on the unwrapped spatial-temporal slice [21]. The impulse SAW phase velocity curve, shown in Figure 6(d), was then estimated based on the k-f domain image through Equation 8. The low and high cut-off frequencies at 0.6 kHz and 0.9 kHz were determined for further analysis of viscocity estimation. The low cut-off frequency was dertermined by 1) ignoring the significant dispersion region from DC to ~0.3 kHz that may attribute to the confined geometry, e.g. the limited lateral distance of the sample [27]. Due to M-B scan protocol, it is easy for the repeatedly-excited forwarding impulse SAW to interfere with remaining-reflected low frequency components of previous impulse SAW, and then generates additional dispersion (on top of the dispersion of the material itself) in the low frequency region; 2) avoiding the overestimated phase velocities and significant disperion region in the low frequency range from ~0.3 kHz to ~0.6 kHz, which was aroused by the overlap between low freqeuncy components of combined mechanical wave and the pure impulse SAW. The high cut-off freqency was dertermined by the typical dispersion behaviour observing frequency of elastic wave in viscoelastic material (e.g. less than 1 kHz [9]), thus, 0.9 kHz was selected in our case. Therefore, only the phase velocity curve in between the low and high cut-off frequency range was kept for further analysis.

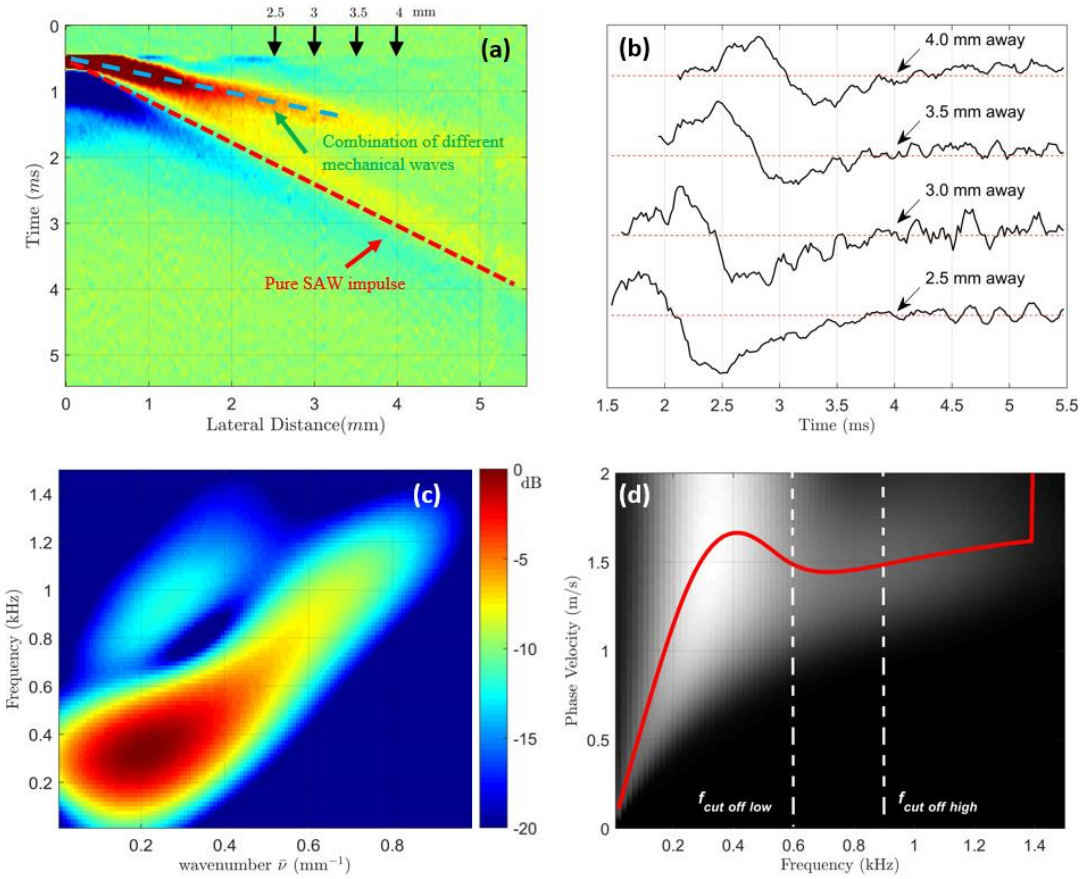

Figure 6. (a) Unwrapped spatial-temporal slice of impulse SAW propagation in a 20% cream-in-agar phantom. (b) Typical impulse SAW waveform (solid black) with baseline (red dashed) in a 20% cream-in-agar phantom at 2.5 mm, 3.0 mm, 3.5 mm and 4.5 mm away from wave source. These locations are also denoted in (a) by black arrows. (c) Impulse SAW k-f domain with color coded intensity (0 ~ -12 dB). (d) Impulse SAW phase velocity curve (solid red) superimposed on gray scale intensity map with low (0.6 kHz) and high (0.9 kHz) cut-off frequency.

4.2. Viscoelastic parameters estimated from impulse SAW experiment

Figure 7 showed the final average impulse SAW phase velocity dispersion curves for all three types of tissue mimicking phantom samples from all experiments. It could be directly seen that the impulse SAW phase velocity curve became more horizontal as the percentage of liquid-paraffin-based cream increases in the sample. The phase velocity increment over the frequency range of 0.3 kHz was: 0.049 m/s for 10% cream-in-agar phantom, 0.015 m/s for 20% cream-in-agar phantom and 0.008m/s for 30% cream-in-agar phantom. A less increment was corresponding to a less dispersion in the impulse SAW and less viscosity in the sample.

The initial phase velocity also changed with the percentage of liquid-paraffin-based cream in the sample, increasing from 1.45 m/s (10% cream-in-agar phantom) to 1.86 m/s (30% cream-in-agar phantom), corresponding to the increasing elasticity in the sample.

Table 1 summarised the estimated shear elasticity μ_1 and shear viscosity μ_2 results from Rayleigh wave dispersion model (Equation 2) for all three different kinds of samples. The model fitting was done by a home-built MATLAB program. The shear elasticity μ_1 increases from 1969.07 ± 83.98 Pa for 10% cream-in-agar phantom to 3793.78 ± 68.70 Pa for 30% cream-in-agar phantom, while the shear viscosity μ_2 decreases from 0.0909 ± 0.0071 Pa·S for 10% cream-in-agar phantom to 0.0070 ± 0.0006 Pa·S for 30% cream-in-agar phantom. The shear elasticity G* in the fourth column of

Table 1 is the shear modulus calculated directly from the group velocity of SAW impulse using pure elastic Rayleigh wave model ($G^* = \rho(\frac{C_R}{0.95})^2$), which can be considered as the elasticity evaluated without taking viscosity into account, while the fifth column shows the relative estimation error of the shear elasticity estimated with and without taking viscosity into account. The relative estimation error reduces from 26.38% in 10% cream-in-agar phantom to 1.48% in 30% cream-in-agar phantom as the viscosity decreases in the phantom.

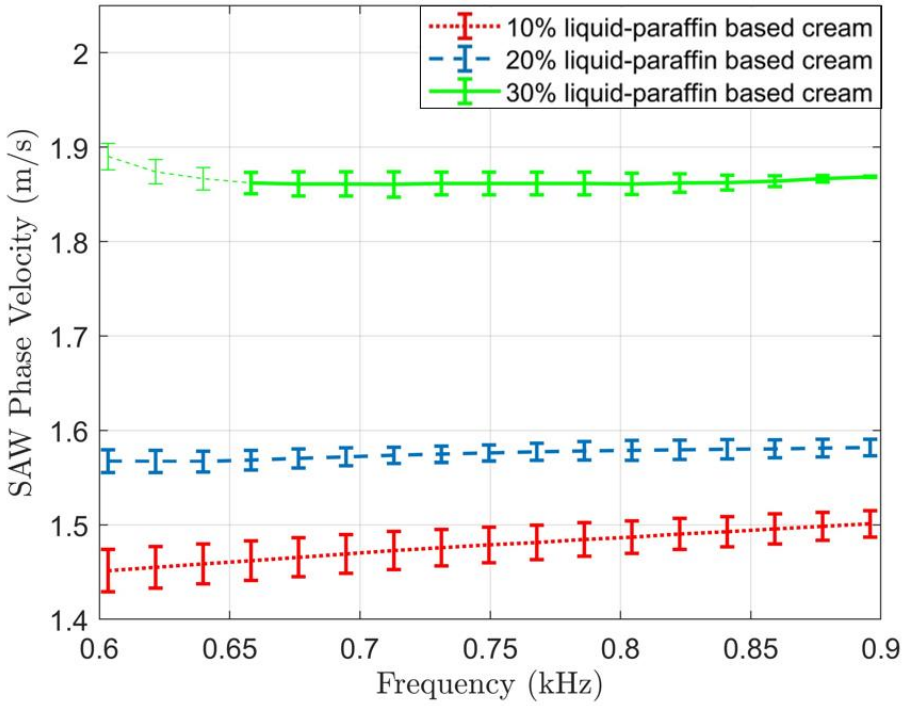

Figure 7. Impulse SAW phase velocity dispersion curves of 10%, 20% and 30% cream-in-agar phantom. The dispersion of surface acoustic wave decreased with concentration of liquid-paraffin-based cream increasing. For 30% cream-in-agar phantom, only solid green part was utilized for viscoelastic parameters estimation.

Table 1. Comparison of shear elasticity μ_1, viscosity μ_2 from SAW dispersion equation and shear elasticity G from group velocity for 10%, 20% and 30% cream-in-agar phantom

Cream Concentration (%)	Shear elasticity μ_1 (Pa)	Shear viscosity μ_2 (Pa·S)	Shear elasticity G* (Pa)	Relative Error (%)
10	1969.07 ± 83.98	0.0909 ± 0.0071	2488.65 ± 81.56	26.38
20	2562.93 ± 45.31	0.0327 ± 0.0091	2748.03 ± 67.72	7.22
30	3793.78 ± 68.70	0.0070 ± 0.0006	3849.86 ± 103.27	1.48

***Shear elasticity G** is calculated from the group velocity of impulse SAW using pure elastic Rayleigh wave model, which can be considered as the elasticity evaluated without taking viscosity into account.

4.3 Viscoelastic parameters estimated from spherical indenter, ramp-hold relaxation test

The spherical indenter, ramp-hold relaxation curves and KVFD model fitting for all three types of tissue mimicking phantoms were shown in the Figure 8. For each experiment curve (dots), there were two parts for each curve: the compression part (from 0 s to 36 s) and the force relaxation part (from 36 s to 300 s). The slope of linear region in compression part increased with the increasing concentration of liquid-paraffin-based cream in the samples. It corresponded to the increasing elasticity of the sample. In contrast, the higher liquid-paraffin-based cream concentration sample loss less stress during the relaxation stage, which means it has less viscosity.

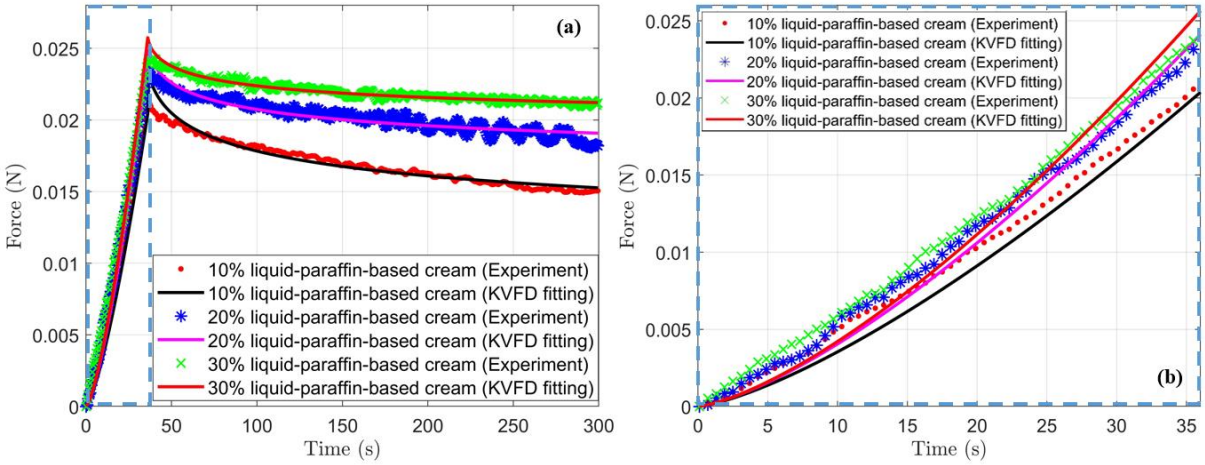

Figure 8. (a) Spherical indenter, ramp-hold relaxation curve for 10%, 20% and 30% cream-in-agar phantom with corresponding KVFD model fitting. The slope of ramp compression part increased with the concentration of liquid-paraffin-based-cream increased, while the slope of relaxation part decreased with the cream concentration increasing. (b) Zoomed figure for only ramp compression part of the experimental data and corresponding KVFD model fitting.

The KVFD model was utilized to analyse the viscoelastic behaviour of the samples. The R-square of all KVFD model fitting were higher than 97% in our study. The fitting results of each parameter in KVFD model for all different samples were summarised in Table 2. Elastic modulus E_0 is the relaxation modulus measured at infinite time. increasing from 2864.30 ± 123.10 Pa for 10% cream-in agar phantom to 7667.40 ± 367.90 Pa for 30% cream-in-agar phantom. The derivative order α is regarded as the sample fluidity ($\alpha \in (0,1)$, 0 for solid, 1 for fluid), also increasing with the liquid-paraffin-based cream precentage increasing from 0.1958 ± 0.0036 to 0.3160 ± 0.0218. The relaxation time constant τ preditcts the time-dependant indentation force relaxation rate, which decrease with the cream precentage incrasing from 769.46 ± 67.17 s to 0.56 ± 0.01 s. Thus, the time-dependent viscosity coefficient η and the normalized time-dependent viscosity η_n also decrease in higher cream concentration sample (10513.08 ± 315.41 Pa·s and 3.68 ± 0.15 s in 10% cream-in-agar phantom, while 6351.19 ± 538.37 Pa·s and 0.83 ± 0.06 s in 30% cream-in-agar phantom).

Table 2. Estimated elastic modulusE_0, derivative order α, relaxation time constant τ, time-dependent viscosity η, normalized time-dependent viscosity η_n and R-square from KVFD model for 10%, 20% and 30% cream-in-agar phantom.

Cream Concentration (%)	Elastic Modulus E_0 (Pa)	Derivative Order α	Relaxation Time Constant τ (s)	Time-dependent Viscosity η (Pa· s)	Normalized Time-dependent Viscosity η_n (s)	R-square (%)
10	2864.30 ± 123.10	0.1958 ± 0.0036	769.46 ± 67.17	10513.08 ± 315.41	3.68 ± 0.15	98.46 ± 0.13
20	5683.66 ± 329.73	0.2352 ± 0.0033	3.37 ± 1.24	7451.87 ± 921.71	1.31 ± 0.13	97.87 ± 0.42
30	7667.40 ± 367.90	0.3160 ± 0.0218	0.56 ± 0.01	6351.19 ± 538.37	0.83 ± 0.06	99.37 ± 0.09

4.4 Discussion

In this paper, characterizing tissue viscoelasticity using the dispersion of impulse SAW was proposed for the purpose of evaluating the viscoelastic parameters of the superficial area of biological tissue, e.g. skin and superficial area of inner organ. Three types liquid-paraffin-based cream-in-agar phantom were used to mimic soft tissues. Two different methods were performed to quantify the viscoelastic properties of these phantoms. In impulse SAW dispersion method, the dispersive SAW phase velocity from 0.6 kHz to 0.9 kHz was chosen to characterize the sample elasticity and viscosity. In spherical indenter, ramp-hold relaxation method, the force-relaxation curve was measured and fitted into KVFD model for obtaining the sample viscoelasticity.

The results from impulse SAW dispersion experiment indicated that increasing the liquid-paraffin-based cream varies the viscoelastic properties of the phantoms (Table 1.). The elasticity increased and viscosity decreased as the cream concentration increases. The results from independent spherical indenter, ramp-hold relaxation experiment confirmed the same trend (Table 2). In addition, the shear wave group velocities in 10% (1.57 ± 0.02 m/s), 20% (1.65 ± 0.02 m/s) and 30% (1.96 ± 0.03 m/s) cream-in-0.5%-agar phantom estimated using time-of-flight method agree well with the same group velocity of 0.5% pure agar phantom in the literature (1.6 m/s) and our previous study (1.8 ± 0.3 m/s) [32-33]. And the viscosity evaluated from impulse SAW dispersion experiment also meets the trend in the literature that the phase velocity is more dispersive in the material with higher viscosity [5, 22, 23]. However, the estimated viscoelasticity from ramp-hold relaxation experiment was larger than that from impulse SAW dispersion experiment. This might be related to the different viscoelastic behaviour of the phantom at different frequency range [5]. The ramp-hold relaxation experiment measured the sample response at almost DC (~0 Hz), while the impulse SAW dispersion experiment measured the sample response at high frequency range (0.6 kHz to 0.9 kHz). The viscous behaviour of the phantom became less at high frequency and typically disappeared at 1 kHz in soft tissue [9]. Therefore, the normalized viscosity from ramp-hold relaxation experiment was larger than the shear viscosity from impulse SAW dispersion experiment. As for the elasticity, the ramp-hold relaxation experiment compressed the sample to 5% stain, but in impulse SAW experiment, the displacement generated by focused ultrasound transducer was only ~0.66 μm (0.12‰ strain), resulting in the deformation of sample being still in the toe region, thus, obtaining smaller elasticity value. However, our experiment could correctly indicate the trend of both elasticity and viscosity.

The advantages of the impulse SAW dispersion method proposed in this paper include: 1) utilizing the impulse SAW that propagates on the air-tissue interface, providing an approach for evaluating the viscoelasticity of the superficial area of biological tissue; 2) taking both elasticity and viscosity of the sample into account. It provides more accurate and unbiased viscoelastic parameters instead of only elasticity (Young's modulus) by our current SAW-OCE method. The estimation error

of shear elasticity increases significantly during mechanical property characterization of viscoelastic material if the viscosity is not considered, which can be seen in Table 1. The fact that elasticity derived from pure elastic model is greater than that from viscoelastic model (Rayleigh wave dispersion equation in our case) also meets the trend in literature 5. By combining shear elasticity and shear viscosity estimated from the proposed method, it is possible to reconstruct the viscosity compensated elastography for displaying both elasticity and viscosity of the sample in one figure, thus provide more useful information for clinical applications. 3) providing the possibility of viscoelasticity characterization using one M-B scan. The impulse SAW phase velocity dispersion curve could be directly extracted from one completed M-B scan. Hence, there is no need to do repeat measurements at different frequencies, which is more suitable for potential clinical translation in the future. One M-scan time for one completed dispersive impulse SAW was 11ms. By using 0.1 kHz pulse repeated frequency shear wave tone bursts, SDUV can also obtain full shear wave dispersion curve using one scan by analysing the harmonic peak in the frequency domain [8]. However, the acquisition time for 0.1 kHz repeated shear wave tone bursts takes 20 to 30 ms for one M-scan.

Nevertheless, there are also some limitations in the proposed impulse SAW dispersion method. The dispersion of the impulse SAW itself will be affected by the confined geometry and other mechanical waves generated at the same time. Therefore, the low frequency part in SAW phase velocity dispersion curve was abandoned in the data processing. The potential solutions for these two problems include: 1) using larger sample to minimize the boundary effects; 2) applying the digital filter on the unwrapped spatial-temporal slice, e.g. Gaussian filter, to reduce the near field effect. The impulse SAW was generated from the back of the sample in a contact way. Thus, this setup could only be applied for ex-vivo clinical applications. However, recently developed air-coupled focus ultrasound transducer makes it possible for generating the impulse SAW in a noncontact way [28]. Therefore, the proposed approach could also be used for in vivo clinical applications by combining noncontact ultrasound transducer. The proposed method in this study is for viscoelastic, isotropic and homogeneous material. While for vertically heterogeneous material (material with different layers, but each layer can be regarded as homogeneous), e.g. skin with layer structure, how to differentiate the dispersion aroused by different layers or the viscosity of the material, and how to evaluate the viscoelastic parameters for each layer still need to be further studied, which will be reported in the following publication.

5. Conclusions

To evaluate the viscoelasticity of the superficial area of biological tissue, the feasibility of using the dispersion of impulse SAW for viscoelasticity characterization of tissue mimicking phantoms was examined in this study. A customized miniature FUS transducer was employed as a impulse SAW inducer, and an M-B mode PhS-OCT system was applied as the wave tracker. Three different types of liquid-paraffin-based cream-in-agar phantom were tested. The phase velocity dispersion curve was extracted using a 2D Fourier transform based phase velocity analysis algorithm. The shear elasticity μ_1 and shear viscosity μ_2 were obtained after fitting the dispersion curve into Rayleigh wave dispersion equation. The results from impulse SAW dispersion method were also compared with that from an independent spherical intender, ramp-hold relaxation test, which showed the same trend in both elasticity and viscosity. Hence, the proposed method has the capability and potential of evaluating the viscoelastic properties of homogeneous soft tissue. By combining shear elasticity and shear viscosity estimated from the impulse SAW dispersion method, it is possible to

reconstruct the viscosity compensated elastography for displaying both elasticity and relative viscosity of the sample in one figure. However, for vertically heterogeneous material, differentiating the dispersion aroused by different layers or the viscosity of the material, and evaluating the viscoelastic parameters for each layer still need to be further studied, which will be reported in the following publication.

References

1. Krouskop TA, Wheeler TM, Kallel F, Garra BS, Hall T. Elastic moduli of breast and prostate tissues under compression. Ultrasonic imaging. 1998 Oct;20(4):260-74.
2. Barry, C.T.; Mills, B.; Hah, Z.; Mooney, R.A.; Ryan, C.K.; Rubens, D.J.; Parker, K.J. Shear wave dispersion measures liver steatosis. *Ultrasound in medicine & biology* 2012, 38, 175-182.
3. Zhang X, Osborn TG, Pittelkow MR, Qiang B, Kinnick RR, Greenleaf JF. Quantitative assessment of scleroderma by surface wave technique. Medical engineering & physics. 2011 Jan 1;33(1):31-7.
4. Kuwahara Y, Shima Y, Shirayama D, Kawai M, Hagihara K, Hirano T, Arimitsu J, Ogata A, Tanaka T, Kawase I. Quantification of hardness, elasticity and viscosity of the skin of patients with systemic sclerosis using a novel sensing device (Vesmeter): a proposal for a new outcome measurement procedure. Rheumatology. 2008 Apr 25;47(7):1018-24.
5. Zhu, Y.; Dong, C.; Yin, Y.; Chen, X.; Guo, Y.; Zheng, Y.; Shen, Y.; Wang, T.; Zhang, X.; Chen, S. The role of viscosity estimation for oil-in-gelatin phantom in shear wave based ultrasound elastography. Ultrasound in medicine & biology 2015, 41, 601-609.
6. Zhang, H.; Wang, Y.; Insana, M.F. Ramp-hold relaxation solutions for the KVFD model applied to soft viscoelastic media. *Measurement Science and Technology* 2016, 27, 025702.
7. Menard, K.P. Dynamic mechanical analysis: A practical introduction. *CRC press*: 2008, 61-72;
8. W Urban, M.; Chen, S.; Fatemi, M. A review of shearwave dispersion ultrasound vibrometry (SDUV) and its applications. *Current medical imaging reviews* 2012, 8, 27-36.
9. Yamakoshi, Y.; Sato, J.i.; Sato, T. Ultrasonic imaging of the internal vibration of soft tissue under forced vibration. *The Journal of the Acoustical Society of America* 1988, 84, S139-S139.
10. Murata H, Shigeto N, Hamada T. Viscoelastic properties of tissue conditioners—stress relaxation test using Maxwell model analogy. Journal of oral rehabilitation. 1990 Jul 1;17(4):365-75.
11. Clayton EH, Garbow JR, Bayly PV. Frequency-dependent viscoelastic parameters of mouse brain tissue estimated by MR elastography. Physics in Medicine & Biology. 2011 Mar 22;56(8):2391.
12. Teodorovich EV. Sliding of a cylinder on a viscoelastic foundation: PMM vol. 42, n≗ 2, 1978, pp. 367–372. Journal of Applied Mathematics and Mechanics. 1978 Jan 1;42(2):384-9
13. Huwart L, Peeters F, Sinkus R, et al. Liver fibrosis: non-invasive assessment with MR elastography. NMR Biomed 2006; 19: 173-9.
14. Mitri, F.G.; Urban, M.W.; Fatemi, M.; Greenleaf, J.F. Shear wave dispersion ultrasonic vibrometry for measuring prostate shear stiffness and viscosity: An in vitro pilot study. *IEEE transactions on biomedical engineering* 2011, 58, 235-242.
15. Hoyt, K.; Castaneda, B.; Zhang, M.; Nigwekar, P.; di Sant'Agnese, P.A.; Joseph, J.V.; Strang, J.; Rubens, D.J.; Parker, K.J. Tissue elasticity properties as biomarkers for prostate cancer. *Cancer Biomarkers* 2008, 4, 213-225.

16. Zhai, L.; Madden, J.; Mouraviev, V.; Polascik, T.; Nightingale, K. In Correlation between SWEI and ARFI image findings in ex vivo human prostates, *Ultrasonics Symposium (IUS), 2009 IEEE International*, 2009; IEEE: pp 523-526.
17. Kemper, J.; Sinkus, R.; Lorenzen, J.; Nolte-Ernsting, C.; Stork, A.; Adam, G. In MR elastography of the prostate: Initial in-vivo application, *RöFo-Fortschritte auf dem Gebiet der Röntgenstrahlen und der bildgebenden Verfahren*, 2004; © Georg Thieme Verlag KG Stuttgart· New York: pp 1094-1099.
18. Amador, C.; Urban, M.W.; Greenleaf, J.F.; Warner, L.V. In Measurements of swine renal cortex shear elasticity and viscosity with shearwave dispersion ultrasound vibrometry (SDUV), *Ultrasonics Symposium (IUS), 2009 IEEE International*, 2009; IEEE: pp 491-494.
19. Li, C.; Guan, G.; Cheng, X.; Huang, Z.; Wang, R.K. Quantitative elastography provided by surface acoustic waves measured by phase-sensitive optical coherence tomography. *Optics letters* 2012, 37, 722-724.
20. Li C, Huang Z, Wang RK. Elastic properties of soft tissue-mimicking phantoms assessed by combined use of laser ultrasonics and low coherence interferometry. *Optics express*. 2011 May 23;19(11):10153-63.
21. Zhou, K.; Le, N.; Huang, Z.; Li, C. High intensity focused ultrasound (HIFU) and phase-sensitive optical coherence tomography (phs-oct) for high resolution surface acoustic wave (SAW) elastography. *Journal of Biophotonics* 2017.
22. Han Z, Singh M, Aglyamov SR, Liu CH, Nair A, Raghunathan R, Wu C, Li J, Larin KV. Quantifying tissue viscoelasticity using optical coherence elastography and the Rayleigh wave model. Journal of biomedical optics. 2016 Sep;21(9):090504.
23. Chen X, Wang Y, Lu J, Li P. Simultaneous viscosity and elasticity measurement using laser speckle fcontrast imaging. Optics letters. 2018 Apr 1;43(7):1582-5.
24. Nenadic, I.Z.; Urban, M.W.; Aristizabal, S.; Mitchell, S.A.; Humphrey, T.C.; Greenleaf, J.F. On lamb and rayleigh wave convergence in viscoelastic tissues. *Physics in medicine and biology* 2011, 56, 6723.
25. Lee S and Knauss W G 2000 A note on the determination of relaxation and creep data from ramp tests Mech. Time-Dependent Mater. 4 1–7
26. Abramowitch S D and Woo S L-Y 2004 An improved method to analyze the stress relaxation of ligaments following a finite ramp time based on the quasi-linear viscoelastic theory J. Biomech. Eng. 126 92–97
27. Friedrich Ch, Sehiessel H and Blumen A 1999 Constitutive behavior modeling and fractional derivatives Rheol. Ser. 12 429–66
28. Koeller R C 1984 Applications of fractional calculus to the theory of viscoelasticity J. Appl. Mech. 51 299–307
29. Wang, R.K.; Kirkpatrick, S.; Hinds, M. Phase-sensitive optical coherence elastography for mapping tissue microstrains in real time. *Applied Physics Letters* 2007, 90, 164105.
30. Robert P., Gerald H. "Guidance for Industry and FDA Staff - Information for Manufacturers Seeking Marketing Clearance of Diagnostic Ultrasound Systems and Transducers", 09 September 2008, https://www.fda.gov/MedicalDevices/ucm070856.htm (2008)
31. Maksuti, E.; Widman, E.; Larsson, D.; Urban, M.W.; Larsson, M.; Bjällmark, A. Arterial stiffness estimation by shear wave elastography: Validation in phantoms with mechanical testing. *Ultrasound in medicine & biology* 2016, 42, 308-321.
32. Zhu J, Yu J, Qu Y, He Y, Li Y, Yang Q, Huo T, He X, Chen Z. Coaxial excitation longitudinal shear wave measurement for quantitative elasticity assessment using phase-resolved optical coherence elastography. Optics letters. 2018 May 15;43(10):2388-91.
33. Song, S., & Huang, Zhihong. (2014). Shear Wave Elastography Based on Optical Coherence Tomography.